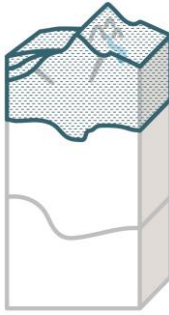




Ambient noise tomography of Australia: application to AusArray deployment

B. Hejrani^{1,2}, R. Hassan¹, A. Gorbatov¹, M. Sambridge², R. Hawkins³, A. Valentine², K. Czarnota¹ and J. Zhao¹

¹Geoscience Australia, ²Australian National University, ³University of Utrecht (the Netherlands)



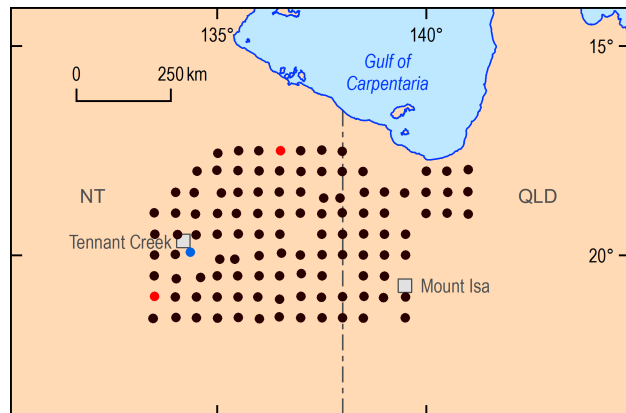
For more than half a century, seismic tomography has been used to map the volumetric structure of Earth's interior, but only recent advances in computation have enabled the application of this technique at scale. Estimates of surface waves that travel between two seismic stations can be reconstructed from a stack of cross-correlations of continuous data recorded by seismometers. Here, we use data from the Exploring for the Future program AusArray deployment to extract this ambient noise signal of Rayleigh waves and use it to image mid- to upper-crustal structure between Tennant Creek and Mount Isa. Our aim was to establish a repeatable, semi-automatic workflow that can be extended to the entire Australian continent and beyond. Shear wave velocity models at 4, 6, 8 and 10 s periods are presented. A strong low-velocity anomaly (2.5 km/s) at a period of 4 s (~2–4 km depth) delineates the outline of the newly discovered, and prospective for hydrocarbons, Carrara Sub-basin. A near-vertical high-velocity anomaly (3.5 km/s) north of Mount Isa extends from the near surface down to ~12 km and merges with northeast-trending anomalies. These elongate features are likely to reflect compositional variations within the mid-crust associated with major structures inferred to be associated with base metal deposits. These outcomes demonstrate the utility of the ambient noise tomography method of imaging first-order features, which feed into resource potential assessments.

For more than a decade, cross-correlations (CC) of continuous background seismic ambient noise have been used to image the crust and mantle structure of Earth through tomographic inversions (e.g. Bensen et al., 2007; Seats et al., 2012). The stack of CC between two stations, the noise correlation function (NCF), is related to Green's function of Earth and hence contains information about its structure. A range of methods have been proposed to calculate NCFs and to extract information about seismic waves that propagate through Earth and are affected by its structure (Ekström et al., 2009; Prieto et al., 2009; Menke and Jin, 2015; Kim et al., 2017; Hawkins and Sambridge, 2019). Ambient noise tomography (ANT) is a powerful tool that exploits these features to image shallow structures. To date, large-scale application of ANT has been hindered by mostly manual procedures of data analysis.

As part of the Exploring for the Future (EFTF) program, a movable seismic array (AusArray) was deployed in stages (Gorbatov et al., 2020a). Here, we present a novel semi-automatic workflow of ANT using data from the first AusArray deployment in the Northern Territory (Figure 1). The resulting velocity models of the crust are important for characterising crustal architecture, which is useful for energy and mineral systems assessments and geophysical inversion for the compositional and thermal structure of the lithosphere (e.g. Skirrow et al., 2019).

Noise correlation functions

Application of NCFs to study Earth's structure has made significant advances since its initial use more than 60 years ago (Aki, 1957; Cox, 1973). Bensen et al. (2007) laid out a widely accepted practical guide to calculate NCFs. More recently, several authors have proposed alternative approaches to enhance the signal in NCFs, applying a wide range of signal processing techniques and their combinations (Ekström et al., 2009; Seats et al., 2012; Kim et al., 2017; Hawkins and Sambridge, 2019). We analysed these methods and observed similar results at frequencies higher than



● AusARRAY seismic station
● Warramunga array broadband station
● Stations BS27 and BZ20
PP-3572-1

Figure 1 119 AusArray seismic stations, shown as black and red triangles. Blue triangle = Warramunga array broadband station. Red triangles = stations BS27 and BZ20; NCFs from these are shown in Figure 3.

0.05 Hz for all these techniques. At frequencies below 0.05 Hz, we observed that the non-linear effect of one-bit normalisation is quite strong, which may adversely affect the signal. We normalised the data in the time domain following Hawkins and Sambridge (2019) and applied spectral whitening to hourly windows with 10% overlap. Our initial assessment of the raw data led to the identification of 12 stations with corrupt data and GPS clock errors (Gorbatov et al., 2020a). We calculated NCFs for 120 sites—119 from AusArray plus WRAB from Warramunga array—using records from vertical components, which resulted in a total of 7140 NCFs. After initial quality control, 6216 pairs were selected. We binned the NCFs based on station separation and chose the NCF with the highest signal-to-noise ratio in each bin to assess the quality of excited surface waves (Figure 2a) where strong and clear arrival of Rayleigh waves is observed.

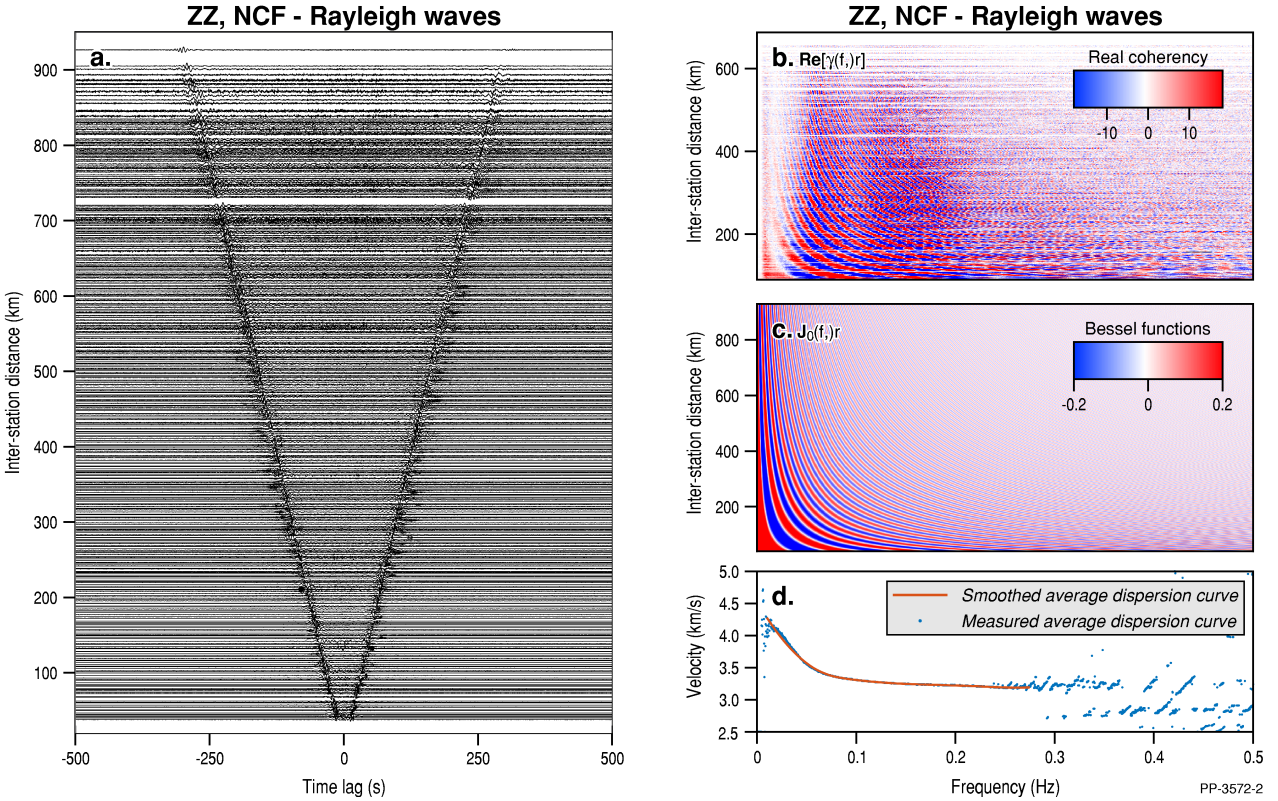


Figure 2 NCFs and procedure for estimating dispersion curves. (a) High-quality NCFs for vertical components (ZZ) binned and plotted in time–distance domain. Rayleigh wave arrivals are visible. (b) Real part of the spectrum of the binned NCFs in the frequency–distance domain, $\text{Re}[\gamma(f, r)]$. (c) Bessel functions in frequency–distance domain, $J_0(f, r)$. Note the similarity with that of NCFs. (d) Estimated average dispersion curve by comparing (b) and (c) following Prieto et al. (2009). Our NCFs show a clear signal within 0.01–0.275 Hz.

Estimation of phase velocity

The traditional method for extracting seismic velocities from surface waves is by manually picking dispersion curves using frequency time analysis (Bensen et al., 2007). This estimates group velocity as a function of frequency. Recently, a range of methods have been proposed to automatically assist the extract of phase velocity from zero crossings of the real part of the spectrum of NCFs (Ekström et al., 2009; Prieto et al., 2009; Menke and Jin, 2015; Kim et al., 2017; Hawkins and Sambridge, 2019). These methods stem from the idea presented by Aki (1957) that the phase velocity of a propagating surface wave could be estimated by expressing the real part of the spectrum of NCFs with Bessel functions:

$$\rho(r, \omega_0) = J_0\left(\frac{\omega_0}{c(\omega_0)}r\right). \quad [1]$$

where $c(\omega_0)$ is the phase velocity at frequency ω_0 and r is station separation. This formula states that the average cross-spectrum $\rho(r, \omega_0)$ varies according to J_0 , the zero-order Bessel function of the first kind. Aki (1957) suggested that, by measuring $\rho(r, \omega_0)$ for a station-pair (separated by distance r) at a range of frequencies, the dispersion curve $c(\omega_0)$ could be estimated using equation 1. Ekström et al. (2009) used Aki's formula to measure dispersion curves for all station-pairs across the USArray (<http://www.usarray.org>). In their study, they only considered fitting the zeros of the Bessel function to the real part of the cross-spectrum, since the amplitude of the spectrum is affected by both the background noise and the non-linear effect of data processing. The location of zeros is less sensitive to the power of the background noise:

$$c(\omega_n) = \frac{\omega_n r}{Z_n} \quad [2]$$

where ω_n is the frequency of the n^{th} observed zero crossings, Z_n is the n^{th} zero of the Bessel function J_0 , and $c(\omega_n)$ is the

phase velocity at that frequency, following equation 1. Quite often, noise in the spectra causes missed or extra zeros, which result in jumps and discontinuities in the measured dispersion curves. Therefore, usually a range of phase velocities are estimated:

$$c_m(\omega_n) = \frac{\omega_n r}{Z_{n+2m}} \quad [3]$$

where m is $0, \pm 1, \pm 2, \dots$, accounting for the number of missed or extra zero crossings. A few methods have been proposed to overcome the irregularities caused by missed or extra zeros. Ekström et al. (2009) selected a dispersion curve if it falls within a realistic range at low frequencies (<0.1 Hz), while its smoothness and continuity are used as quality criteria at higher frequencies (>0.1 Hz). Prieto et al. (2009) proposed estimating an average phase velocity below a seismic array. In this approach, the real part of the spectrum of all (or a subset of) NCFs is compared with the Bessel function of first kind in a frequency–distance domain. The result is an average dispersion curve beneath an array of stations. This is a fast, efficient and data-driven approach to estimate the average dispersion curve, compared with the traditional approach of using reference 1D Earth models. The average dispersion can guide the selection of outliers and irregularities in the dispersion curves. In a recent paper, Hawkins and Sambridge (2019) proposed a two-stage method to obtain a smooth and stable dispersion curve. First, the phase velocity dispersion curves are estimated from zero crossings, together with the peaks and troughs of the NCF spectrum. Then a second step finds a 1D path average Earth model to accurately fit the NCF. This second step acts as a constraint that allows inversion for both Love and Rayleigh dispersion curves.

In this study, we present the combination of three approaches. First, the method of Prieto et al. (2009) was

used to estimate an average phase velocity dispersion curve and identify the frequency band where our dispersion curves show patterns similar to that of Bessel functions (Figure 2b, c). We observe a stable dispersion curve at 0.01–0.275 Hz (Figure 2d). At this frequency band, the sinusoidal patterns in the real part of the spectra follow the Bessel functions, which result in a smooth average dispersion curve. Then, for each station-pair, a phase velocity dispersion curve following Ekström et al. (2009) and Hawkins and Sambridge (2019) was obtained. Figure 3 shows an example of a dispersion curve measurement for the station-pair BS27 and BZ20 (red triangles in Figure 1). In this example, a strong signal is observed in the expected window. We observe the same signal-to-noise ratio for all station-pairs that are oriented perpendicular to the southwest-trending coastline of the Gulf of Carpentaria (Figure 1). For station-pairs that are oriented parallel to the Gulf, we observe a strong signal at 0.1–0.25 Hz (the second microseismic noise band) between the causal and acausal parts of the trace, which is generated at the continental shelf around the Gulf of Carpentaria.

We applied a quality control before extraction of dispersion curves by measuring the ratio of maximum amplitude within a ‘signal’ window (orange waveform in Figure 3a) to the maximum amplitude of the rest of the trace (blue waveform in Figure 3a). The signal window was chosen using extreme values for minimum and maximum velocity of surface waves in the shallow crust (1 km/s) and the upper mantle (5.5 km/s), for both causal and acausal parts of the trace. We then collected dispersion curves from NCFs with a signal-to-noise ratio larger than 2, which results in a total of 4269 station-pairs. Finally, estimated dispersion curves were used to derive 2D tomographic maps of Rayleigh wave phase velocity beneath the first AusArray deployment (Figure 2). Developed algorithms and workflow significantly reduced the need for manual processing—and consequently costs—allowing passive imaging on a large scale for the purpose of minerals and energy systems assessments.

Ambient noise tomography

ANT has been used to image the lithospheric structure of Earth at a wide range of resolutions (e.g. Saygin and Kennett, 2010). Our current ray coverage provides 1° (~111 km) lateral resolution, which could be improved to at least 0.5° with time. We use the subspace fast marching surface tomography method (Rawlinson and Sambridge, 2005) to invert the travel times for a set of 2D tomographic models.

We present four 2D tomographic images, at 4, 6, 8 and 10 s periods (Figure 2). The result of inversion at the 4 s period, which reflects shallow layers of the crust (2–4 km depth), shows a strong negative anomaly. This anomaly corresponds with a negative Bouguer gravity anomaly and helps to delineate the distribution of the newly discovered Paleo to Mesoproterozoic Carrara Sub-basin of the South Nicholson Basin (Carr et al., 2020). This sub-basin was imaged as part of the EFTF program by deep reflection seismic profiles and has potential to host new hydrocarbon resources (Carr et al., 2020; Fomin, et al., 2020). This negative anomaly disappears at longer periods that are sensitive to greater depths.

We also observed a strong high-velocity anomaly north of Mount Isa, which could be associated with more mafic rocks. This anomaly is visible down to a period of 10 s (~12 km depth) and merges with east–west to northeast–southwest-striking positive anomalies at these depths. The trend of these features corresponds with major structures imaged across the Tennant Creek to Mount Isa region and second-order variations in crustal thickness (Gorbatov et al., 2020b; Schofield et al., 2020).

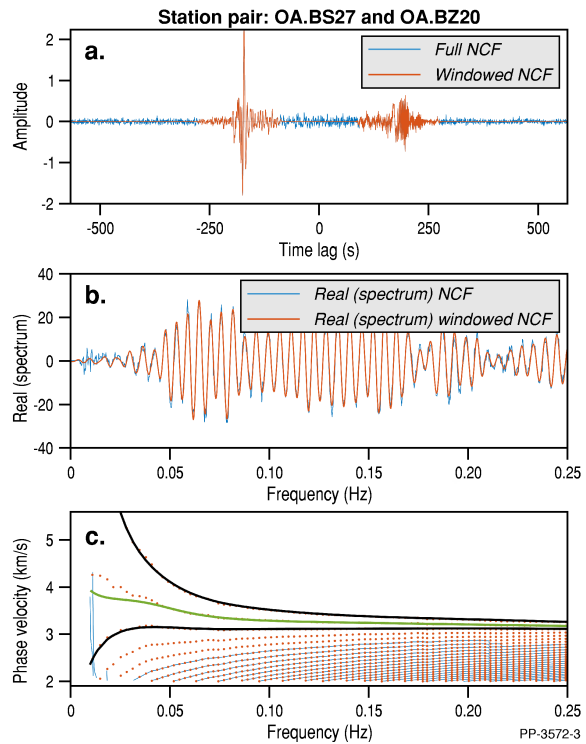


Figure 3 Example of dispersion curve extraction. (a) NCF for BS27 and BZ20 (blue) and the signal window (orange). (b) Real part of the spectrum for full trace (blue) and the signal (orange). (c) Phase velocity dispersion curves calculated by fitting the zeros of Bessel function to full trace (blue curves) and signal (orange dots). The range of curves corresponds to different ‘ m ’ in equation 3. The thick black lines show one cycle around the average dispersion curve obtained in Figure 2. The green curve is the estimated dispersion curve from Hawkins and Sambridge (2019).

Major base metal deposits appear to be associated with the edges of these positive anomalies, and the structure east of Tennant Creek has been inferred to be prospective for iron oxide–copper–gold mineralisation (Schofield et al., 2020). There is also a northwest-striking feature around Tennant Creek. These relationships show that ANT places first-order architectural constraints, useful for both mineral and energy assessments in frontier regions.

Conclusions

We have developed a novel semi-automatic workflow for seismic ANT. This is part of the HiPerSeis code, which is freely available as an open-source package through our [GitHub repository](#), under the GNU GPLv3 licence (Hassan et al., 2020). Newly developed routines allow quick and efficient automatic data processing. These advances enable processing of large datasets for high-resolution ANT by removing the need for human intervention, which reduces analysis costs and positions the workflow for uptake by explorers and scientists.

Images from our tomographic inversions constrain crustal architecture, which is important for resource potential assessments. For example, we imaged a low-velocity anomaly at shallow depths that delineates volumetrically the extent of the newly discovered, and prospective for hydrocarbons, Carrara Sub-basin. Stripped velocity anomalies in the mid-crust likely reflect crustal composition variations controlled by major structures, which may be associated with base metal and gold mineralisation. Further ANT insights from AusArray are expected as our work provides a foundation for higher-resolution models.

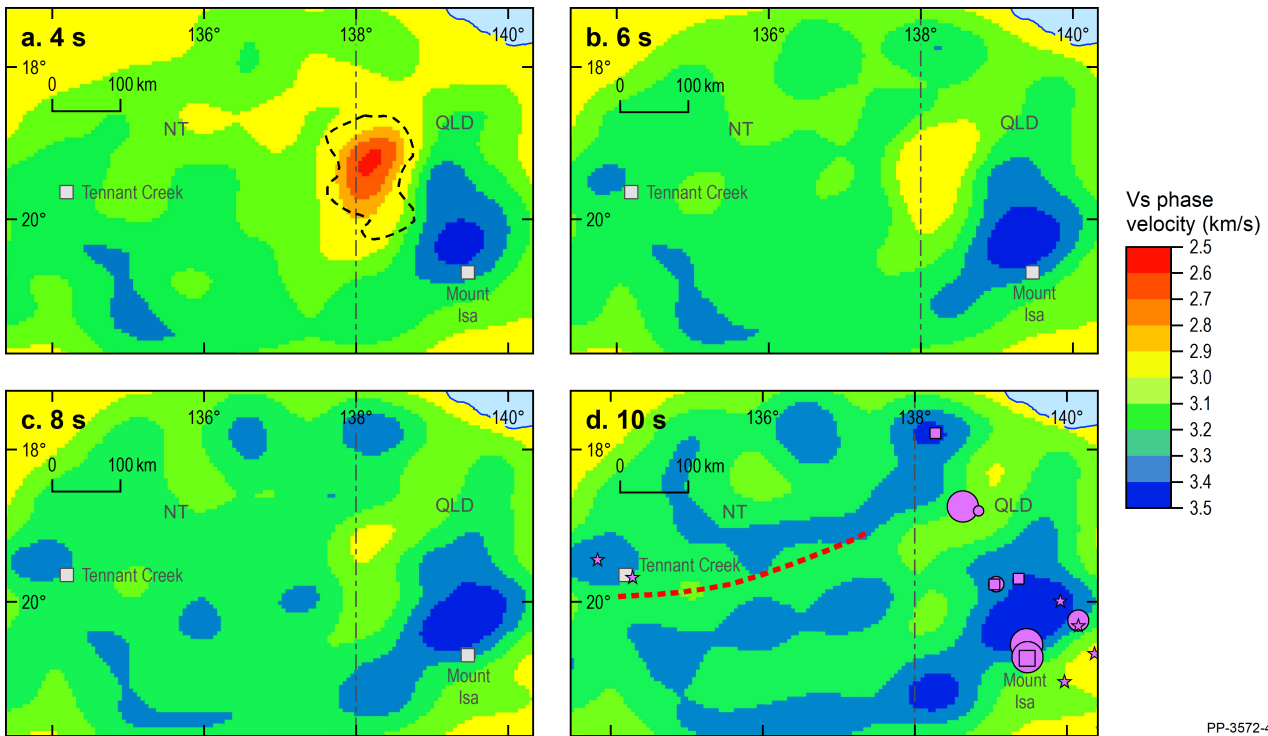


Figure 2 Tomographic maps of Rayleigh wave phase velocity (V_s) beneath AusArray deployment at (a) 4 s (~2–4 km depth), (b) 6 s, (c) 8 s and (d) 10 s (~10–12 km depth) periods. In (a), black dashed line = Carrara Sub-basin outlined by Carr et al. (2020). In (d), red dashed line = inferred step in the Moho from Schofield et al. (2020). Pink circles, square and stars = Zn-Pb, Cu and iron oxide-copper-gold, respectively. Deposits are scaled by contained metal: small = <1 Mt; medium = 1–10 Mt; large = >10 Mt, respectively from Hoggard et al. (in press).

PP-3572-4

Acknowledgements

Y. Lee-Cooper and R. Costelloe reviewed the manuscript. This abstract is published with the permission of the CEO of Geoscience Australia.



© Commonwealth of Australia (Geoscience Australia) 2019
eCat: 135130, doi: [10.11636/135130](https://doi.org/10.11636/135130)

References

- Aki K., 1957. Space and time spectra of stationary stochastic waves with special reference to microtremors. *Bulletin of the Earthquake Research Institute* 35:415–56.
- Bensen G. D., et al., 2007. Processing seismic ambient noise data to obtain reliable broad-band surface wave dispersion measurements. *Geophysics Journal International* 169:1239–60.
- Carr L., et al., 2020. South Nicholson Basin seismic interpretation. In: Czarnota K., et al. (eds.), *Exploring for the Future: extended abstracts*, Geoscience Australia, 1–4.
- Cox H., 1973. Spatial correlation in arbitrary noise fields with applications to ambient sea noise. *Journal of the Acoustic Society of America* 54:1289–1301.
- Ekström G., Abers G. A. & Webb S. C., 2009. Determination of surface-wave phase velocities across USArray from noise and Aki's spectral formulation. *Geophysical Research Letters* 36:L18301.
- Fomin T., Holzschuh J., Costelloe R. D. & Henson P., 2020. Deep northern Australian 2D seismic reflection surveys. In: Czarnota K., et al. (eds.), *Exploring for the Future: extended abstracts*, Geoscience Australia, Canberra, 1–4.
- Gorbatov A., et al., 2020a. AusArray: towards updatable, national high-resolution seismic velocity models of the lithosphere. In: Czarnota K., et al. (eds.), *Exploring for the Future: extended abstracts*, Geoscience Australia, Canberra, 1–4.
- Gorbatov A., et al., 2020b. Moho variations in northern Australia. In: Czarnota K., et al. (eds.), *Exploring for the Future: extended abstracts*, Geoscience Australia, Canberra, 1–4.
- Hassan R., Hejrani B., Medlin A., Gorbatov A. & Zhang F., 2020. High-performance seismological tools (HiPerSeis). In: Czarnota K., et al. (eds.), *Exploring for the Future: extended abstracts*, Geoscience Australia, Canberra, 1–4.
- Hawkins R. & Sambridge M., 2019. An adjoint technique for estimation of interstation phase and group dispersion from ambient noise cross correlations. *Bulletin of the Seismological Society of America* 109:1716–28.
- Hoggard M. J., et al., in press. Global distribution of sediment-hosted metals controlled by craton edge stability. *Nature Geoscience*.
- Kim S., Tkalcic H. & Rieh J., 2017. Seismic constraints on magma evolution beneath Mount Baekdu (Changbai) volcano from transdimensional Bayesian inversion of ambient noise data. *Journal of Geophysical Research: Solid Earth* 122:5452–73.
- Menke W. & Jin G., 2015. Waveform fitting of cross spectra to determine phase velocity using Aki's formula. *Bulletin of the Seismological Society of America* 105:1619–27.
- Prieto G. A., Lawrence J. F. & Beroza G. C., 2009. Anelastic earth structure from the coherency of the ambient seismic field. *Journal of Geophysical Research* 114:B07303.
- Rawlinson N. & Sambridge M., 2005. The fast marching method: an effective tool for tomographic imaging and tracking multiple phases in complex layered media. *Exploration Geophysics* 36:341–50.
- Saygin E. & Kennett B. L. N., 2010. Ambient seismic noise tomography of Australian continent. *Tectonophysics* 481:116–25.
- Seats K. J., Lawrence J. F. & Prieto G. A., 2012. Improved ambient noise correlation functions using Welch's method. *Geophysical Journal International* 188:513–23.
- Schofield A., et al., 2020. Data integration for greenfields exploration: an example from the East Tennant region, Northern Territory. In: Czarnota K., et al. (eds.), *Exploring for the Future: extended abstracts*, Geoscience Australia, Canberra, 1–4.
- Skirrow R. G., et al., 2019. Mapping iron oxide Cu-Au (IOCG) mineral potential in Australia using a knowledge-driven mineral systems-based approach. *Ore Geology Reviews* 113:103001.